

*Post-print of the article published on:
Chem. Eng. Res. Des. (2014)*

Please cite this article in press as: Tedesco, M., et al., A simulation tool for analysis and design of reverse electro dialysis using concentrated brines. Chem. Eng. Res. Des. (2014), <http://dx.doi.org/10.1016/j.cherd.2014.05.009>

A simulation tool for analysis and design of Reverse Electro dialysis using concentrated brines

Michele Tedesco^a, Andrea Cipollina^{a}, Alessandro Tamburini^a, I. David L. Bogle^b,
Giorgio Micale^a*

^aDipartimento di Ingegneria Chimica, Gestionale, Informatica, Meccanica (DICGIM), Università di Palermo (UNIPA) – viale delle Scienze Ed.6, 90128 Palermo, Italy. *e-mail: michele.tedesco@unipa.it, andrea.cipollina@unipa.it

^bCentre for Process Systems Engineering, Department of Chemical Engineering, UCL (University College London), London WC1E 7JE, United Kingdom

Abstract

Reverse Electro dialysis (SGP-RE or RED) represents a viable technology for the conversion of the Salinity Gradient Power into electric power.

A comprehensive model is proposed for the RED process using sea or brackish water and concentrated brine as feed solutions. The goals were (i) reliably describing the physical phenomena involved in the process and (ii) providing information for optimal equipment design. For such purposes, the model has been developed at two different scales of description: a lower scale for the repeating unit of the system (*cell pair*), and a higher scale for the entire equipment (*stack*).

The model was implemented in a process simulator, validated against original experimental information and then used to investigate the influence of the main operating factors and on power output. Feed solutions of different salinities were also tested. A good matching was found between predictions and experiments for a wide range of inlet concentrations, flow rates and feed temperatures. Optimal feed conditions, for the adopted system geometry and membranes, have been found employing brackish water (0.08-0.1 M NaCl) as dilute and brine (4.5-5 M NaCl) as concentrate to generate the highest power density at 40°C temperature.

The model can be used to explore the full potential of the RED technology, especially for any investigation regarding the future scale-up of the process.

Keywords

Salinity Gradient Power; Reverse Electro dialysis; sea water; brine; process simulator; multi-scale model.

1 Introduction

The importance of exploring renewable sources of energy, both for environmental issues and for reducing our dependence from fossil fuels, has already been broadly discussed and accepted. In this context, a promising energy source almost equally distributed worldwide is Salinity Gradient Power (SGP), i.e. the energy available from mixing two aqueous solutions at different salinity. The success in collecting this chemical energy and convert it into a more exploitable form is related to managing the mixing in suitably controlled conditions. Up to now, three different technologies have been proposed in the literature: Reverse Electrodialysis (RE or RED) [1, 2], Pressure Retarded Osmosis (PRO) [3] and Capacitive Double Layer Expansion (CDLE) [4]. The first two are membrane-based technologies, in which the controlled mixing is achieved by the use of suitable membranes acting as semi-permeable barriers, thus allowing the transport of either ions (RED) or water (PRO). Although both of them are promising processes and many efforts are being made in research and development, RE has, in fact, a remarkable advantage with respect to PRO: in this latter, SGP is converted first into pressure/mechanical energy and, then, into electrical energy by means of hydroelectric turbines; RED, conversely, being an electrochemical process allows the direct conversion of SGP into electric energy. Moreover, the use of concentrated brines would lead in a PRO system to very high osmotic pressure differences, which would be difficult to handle with available osmotic membranes, whereas high brine concentrations will increase the power generation in RED systems.

Recently other electrochemical processes have been proposed, which are based on the capacitive properties of porous electrodes immersed alternatively in high/low concentrated solution (CDLE) [4], possibly combined with ion exchange membranes in a flow cell [5]. However, these technologies, whose bottleneck is essentially the development of suitable electrode materials, are still in their very early R&D stage.

The principle of RED is sketched in Figure 1. The repeating unit of the system (*cell pair*) is constituted by a Cation Exchange Membrane (CEM), a dilute compartment, an Anion Exchange Membrane (AEM) and a concentrate compartment. In practical applications, up to several hundreds of cell pairs can be stacked in a single unit. Polymeric net spacers are normally used to maintain the inter-membranes distance, as well as for reducing concentration polarisation phenomena. At the ends of the cell pairs stack the external compartments contain the electrodes and an electrolyte solution (*electrode rinse solution*) with a suitable redox couple (e.g. $\text{Fe}^{2+}/\text{Fe}^{3+}$ chloride).

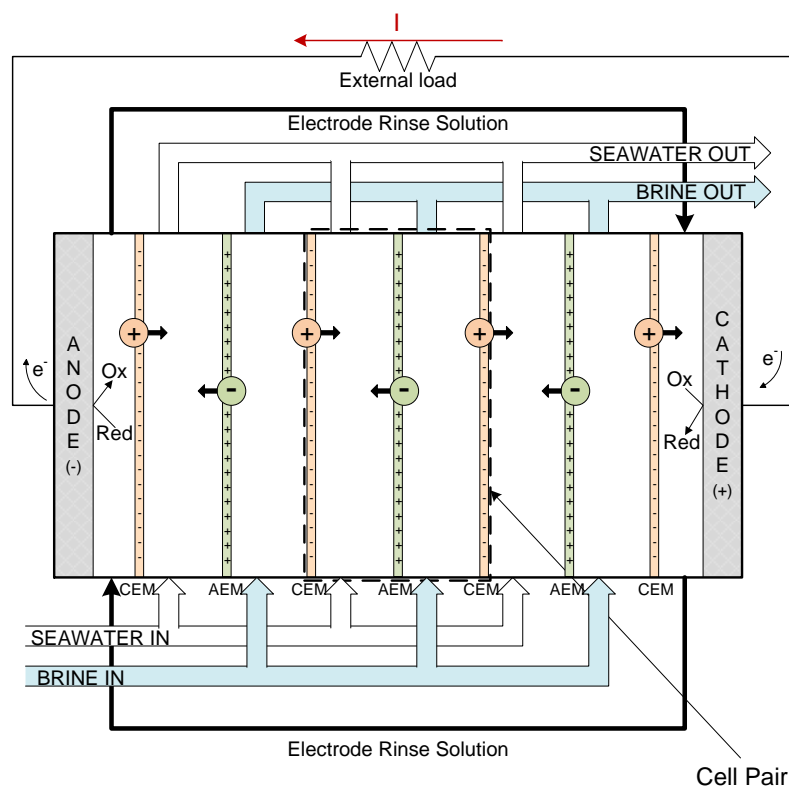


Figure 1. Principle of the RED process.

When two salt solutions are fed to the stack, the concentration gradient between them generates the ion movement through the membranes. This ion flux is regulated by the membrane permselectivity, i.e. the selectivity towards cation/anion transport through CEM/AEM, respectively: ideally, only cations flow through CEMs, as well as anions through AEMs (in the opposite direction). Finally, this ionic current through membranes is converted into electric current by means of redox reactions at the electrodes and can be collected by an external load.

The RED process has been described as a promising technology in the literature since 1954 [1, 2, 6, 7]; most recently Veerman *et al.* obtained a power of 0.93 W with a 50 cell pairs stack of 1 m² of total membrane area, using river water and seawater as feed solutions [8]. The use of river water has in fact a remarkable drawback: the low conductivity of the solution provokes high internal ohmic losses within the unit, limiting the output power achievable. For this reason, decreasing the compartments' thickness can reduce considerably the stack resistance, so as to enhance the output power: for instance, Vermaas *et al.* reported a power density of 2.2 W/m² of membrane using spacers of 60 μm thickness [9]. Another possibility to avoid high resistance in the dilute compartment is using brackish or sea water (instead of river water) as dilute, and a more concentrated solution as concentrate, such as concentrated brine from saltworks, salt mines or other industrial activities [10-12].

The earliest modelling works on RED process [6, 13] were based on theoretical estimation of the relevant electric variables of the system (such as voltage and output power), providing just a rough estimate of the technical feasibility of the process. The first comprehensive modelling work was proposed by Lacey [1], who took into account the potential drops through bulk solutions, boundary layers and IEMs for estimating the cell pair voltage. Brauns [14], modifying Lacey's model, investigated the effect of specific parameters on process efficiency: he pointed out how the development of thinner Ionic Exchange Membranes (IEMs), up to values <10 μm, may enhance significantly the process

performances. Finally, Veerman *et al.* [15] proposed a cell pair model based both on thermodynamic equations for voltage calculation and transport equations through IEMs, taking into account the effect of spacer on electric resistance and the non-ideal behaviour of IEMs.

The first models were only simplified approaches for the estimation of the main process performance parameters, using lumped variables and considering only ideal behaviour of all system components. The more recent model presented by Veerman *et al.* was developed for river water and seawater as feed solutions, failed to predict the behaviour of the system in a wider range of operating conditions due to some simplifying assumptions and constitutive equations valid only in a limited concentration range. In fact, using higher salt concentration within the system can affect both membranes and solutions behaviour, increasing the complexity of the physical/mathematical description of the process.

A recent model, based also on Veerman's approach, was developed by Tedesco *et al.* [16], in which the authors attempted to extend the previous model to a wider range of concentration, giving a more general validity to the simulation tool developed. However, a number of non-ideal effects were still neglected in this latter model, such as the water transport through membranes (both osmotic and electro-osmotic fluxes), concentration polarisation phenomena and the presence of parasitic currents through manifolds.

The focus of this work has been to develop a comprehensive model for the RED process using sea or brackish water and concentrated brine. The model has been developed starting from the work developed by the same authors [16] and improving the prediction capability also for non-ideal phenomena previously neglected.

The modelling goals are (i) reliably describing the physical phenomena involved in the process and (ii) providing information for optimal equipment design. For these purposes, the model has been developed at two different scales of description: a lower scale (*cell pair*), for the repeating unit of the system and a higher scale (*stack*) for the entire equipment. After model validation via experimental data collected on lab-scale equipment, the model was implemented into a process simulator (gPROMS®) in order to develop a simulation tool able to predict the system performance under different operating conditions (feed solutions flow rate, temperature and concentration) as well as process parameters (spacer thickness, number of cell pairs, etc.).

The next section presents the model and its assumptions; section 3 describes the experimental activities carried out for model calibration, as well as the validation procedure; the relevant results predicted by the model are reported in section 4. Finally, section 5 summarises the main conclusions achieved.

2 Model Development

In order to match the aforementioned modelling goals, the RED system was modelled at two different scales of description (Figure 2):

- a low-hierarchy scale (*cell pair*), describing the physical phenomena inside the repeating unit of the RED system;
- a high-hierarchy scale (*stack*) for the entire equipment, describing the interactions among all cell pairs and providing information on the performance of the equipment.

The cell pair model proposed by Veerman *et al.* [15] and, then, by Tedesco *et al.* [16] for the RED process was adopted as starting point for the lower scale modelling.

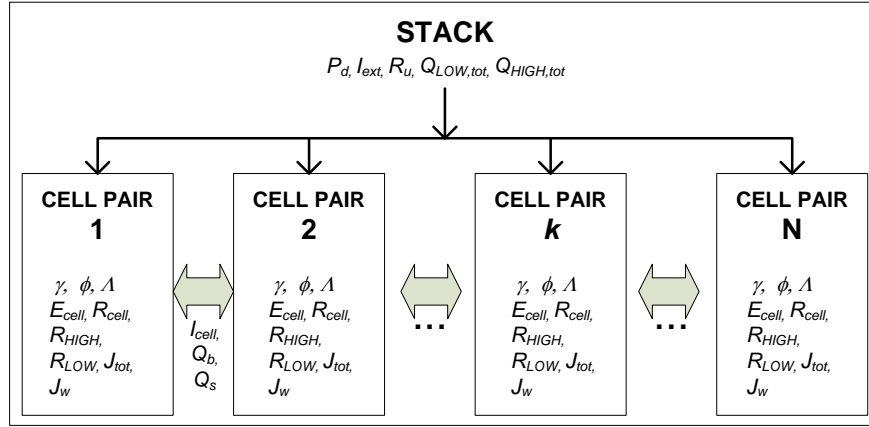


Figure 2. Structure of the proposed model.

2.1 Low-hierarchy model (*cell pair*)

The modelling approach first focused on the repeating unit of the stack (*cell pair*, Figure 3). The following assumptions have been made in order to build the model:

- a) A co-current flow distribution is assumed.
- b) The computational domain is discretised along the flow path length, thus calculating the variation of solutions properties along this direction
- c) Both streams are modelled as purely sodium chloride aqueous solutions, i.e. disregarding the other ions usually present in real seawater/brine.
- d) Parasitic currents within the electrode rinse solution circuit are negligible. This hypothesis has been fully verified, provided that the pipe used for the recirculation of electrode rinse solution (acting as the “salt bridge” allowing the generation of parasitic currents from the high potential to the low potential electrode compartment) is long enough for increasing the electric resistance in the hydraulic circuit [17].

At this level of description, a distributed model has been implemented. In fact, the main variables of the system (solution conductivity, cell pair voltage, etc.) are functions of salt concentration and vary along the channel length (L), due to the mass transport from concentrate to dilute compartment through membranes.

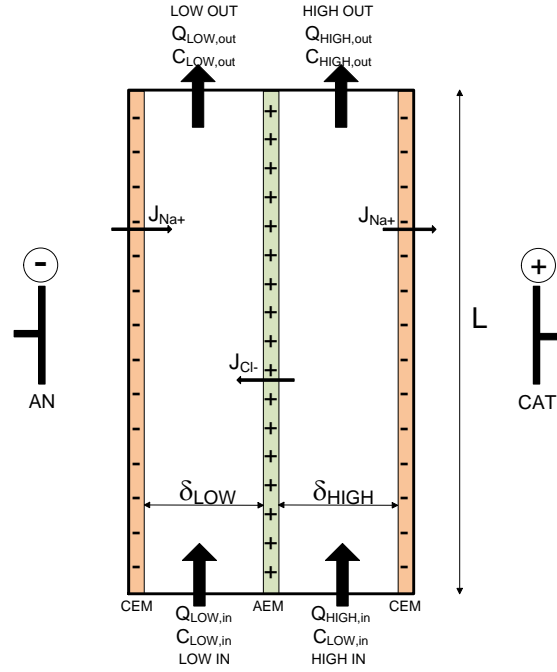


Figure 3. Repeating unit of a RED stack (Cell Pair). A cell pair is constituted by: a Cation Exchange Membrane (CEM), a dilute (sea or brackish water) compartment, an Anion Exchange Membrane (AEM) and a concentrate (brine) compartment.

2.1.1 Thermodynamic properties of solutions

It is worth noting that the high salt concentration affects significantly the physical behaviour of an electrolyte solution. For this reason, the relevant thermodynamic properties of concentrated NaCl solutions were estimated through appropriate correlations from literature. In particular, both activity (γ_{\pm}) and osmotic (φ) coefficients were calculated using Pitzer's virial equations [18]:

$$\ln\gamma_{\pm} = -A_1 \left[\frac{\sqrt{I'}}{1+b'\sqrt{I'}} + \frac{2}{b'} \ln(1+b'\sqrt{I'}) \right] + mB^{\gamma} + m^2C^{\gamma} \quad (1)$$

$$\varphi - 1 = -A_1 \frac{\sqrt{I'}}{1+b'\sqrt{I'}} + mB^{\varphi} + m^2C^{\varphi} \quad (2)$$

where I' and m are the ion strength and molality of the electrolyte, respectively; A_1 is the modified Debye-Hückel constant ($A_1 = 0.3915$ at 25°C), and b' is a constant ($b' = 1.2$ for 1:1-valence electrolyte); the other virial coefficients in eqs. (1) and (2) ($B^{\gamma}, C^{\gamma}, B^{\varphi}, C^{\varphi}$) are only functions of the nature of the electrolyte and have been already evaluated for the most common electrolytes. Their definitions have been reported in the Appendix.

The salt concentration affects also the equivalent conductivity of solutions; this term was estimated for both seawater and brine through a correlation proposed by Islam *et al.* [19]:

$$\Lambda(x) = \left[\Lambda^0 - \frac{B'_2(c)\sqrt{c}}{1+B'(c)a\sqrt{c}} \right] \left[1 - \frac{B'_1(c)\sqrt{c}}{1+B'(c)a\sqrt{c}} F'(c) \right] \quad (3)$$

where Λ^0 is the equivalent conductivity of NaCl at infinite dilution and c is the molar concentration. The other terms in eq. (3) (whose definition can be found in Appendix), are in fact a function of concentration as well as of other solution properties (viscosity and dielectric constant). For these properties, a linear variation with the concentration was assumed within the model, which is well accepted in the literature [20].

2.1.2 Electric variables

The cell pair voltage, arising from a potential difference across each membrane, can be evaluated from the Nernst equation [21]:

$$E_{cell}(x) = \alpha_{CEM} \frac{RT}{F} \ln \frac{\gamma_{HIGH}^{Na}(x) C_{HIGH}(x)}{\gamma_{LOW}^{Na}(x) C_{LOW}(x)} + \alpha_{AEM} \frac{RT}{F} \ln \frac{\gamma_{HIGH}^{Cl}(x) C_{HIGH}(x)}{\gamma_{LOW}^{Cl}(x) C_{LOW}(x)} \quad (4)$$

here R , T , and F have their usual meaning, α_{AEM} , α_{CEM} are the permselectivity of both IEMs [22], and the subscripts *HIGH* and *LOW* are referred to concentrate and dilute solutions, respectively.

The electrical resistance of a cell pair is given by the sum of the resistances through solutions and membranes:

$$R_{cell}(x) = R_{HIGH}(x) + R_{LOW}(x) + R_{CEM,eff} + R_{AEM,eff} \quad (5)$$

where R_{HIGH} and R_{LOW} are the electrical resistances of concentrate and dilute compartments respectively, while $R_{CEM,eff}$ and $R_{AEM,eff}$ are the membrane resistances inside the stack. The solution resistances are evaluated as a function of salt concentration by eq. (6,7):

$$R_{HIGH}(x) = f_y \frac{\delta_{HIGH}}{\Lambda_{HIGH}(x) C_{HIGH}(x)} \quad ; R_{LOW}(x) = f_y \frac{\delta_{LOW}}{\Lambda_{LOW}(x) C_{LOW}(x)} \quad (6,7)$$

where δ_{HIGH} , δ_{LOW} are the two compartments thicknesses and f_y (*shadow factor*) is a geometric constant which accounts for the increase of electrical resistance due to the presence of a non-conductive spacer inside the channels, as will be described in paragraph 2.2.1.

When piled into a stack, membranes are in contact with two different solutions, which affect their electrical resistance. For this reason, the effective electrical resistance of membranes was evaluated as:

$$R_{AEM,eff} = f_m R_{AEM} \quad R_{CEM,eff} = f_m R_{CEM} \quad (8,9)$$

where R_{CEM} and R_{AEM} are the IEMs nominal electrical resistance measured in standardised condition (in this case for 0.5 M NaCl and 4 M NaCl solutions at 25°C in a six-compartments setup [23]), and f_m (*resistance correction factor*) is a correction factor to predict the practical resistances of membranes in process conditions, as will be discussed in paragraph 3.3.

It is worth noting that the electric current density through membranes, which is a variable related to all cell pairs, has been declared in the higher hierarchy model (paragraph 2.2.3) in order to integrate the relevant equations also with the model for parasitic currents.

2.1.3 Salt transport through IEMs

In the ideal case of 100% selective membranes, only counter-ions (ions with opposite charge to the fixed ionic charges in the membrane) are allowed to pass through each IEM. In fact, a real IEM cannot completely reject the co-ions (i.e. ions with the same sign as the fixed charges), especially when highly concentrated solutions are used (as those considered in this work). Therefore, in real conditions co-ions will also pass through membranes to some extent. The salt flux (expressed as NaCl molar flux per cell pair area) outgoing from a concentrate compartment to the closest dilute compartments is evaluated as the sum of counter-ion and co-ion transport through both IEMs [15]. Counter-ion flux can be related to the net ions flux related to the current density (Na^+ through the CEM and Cl^- through the AEM), plus the counter-ion flux coupled with co-ions flux, which, conversely, do not generate any net electrical current (being related to the movement of a neutral salt). This can be expressed as the total salt flux according to:

$$J_{tot}(x) = \frac{j(x)}{F} + 2 \frac{D_{NaCl}}{\delta_m} [C_{HIGH}(x) - C_{LOW}(x)] \quad (10)$$

where j is the ionic current density, being converted into a NaCl molar flux through the two membranes by dividing for the Faraday constant; δ_m is IEMs thickness (assumed equal for AEM and CEM) and D_{NaCl} is the salt permeability coefficient, i.e. a coefficient taking into account ions diffusivity within the membrane and the solution-membrane ion distribution coefficient for both AEM and CEM [22]. The factor 2 accounts for the two IEMs in a cell pair.

Regarding the coupled counter/co-ion flux, the permeability coefficient, D_{NaCl} , has been set to a constant value of $10^{-12} \text{ m}^2/\text{s}$ worked out from literature information. A sensitivity analysis focused on the choice of this parameter will be shown in Figure 13.

2.1.4 Water transport through IEMs

The water transport through membranes is due to two opposite contributions: (i) the osmotic flux (opposite to the salt flux) and (ii) the electro-osmotic flux, in the direction of salt transport and essentially due to the solvent molecules firmly bound in hydration shells. The first term was estimated evaluating the real osmotic pressure difference across each membrane:

$$J_{osm}(x) = -2L_p \Delta\Pi^* = -2L_p \left[\nu RT (\phi_{HIGH} C_{HIGH}(x) - \phi_{LOW} C_{LOW}(x)) \right] \quad (11)$$

where L_p is the water permeability coefficient of IEMs, $\Delta\Pi^*$ is the real osmotic pressure difference and $\varphi_{HIGH}, \varphi_{LOW}$ are the osmotic coefficients for concentrate and dilute solution, respectively (eq. (2)).

The electro-osmotic flux was calculated assuming a total hydration number (n_h) for Na^+ and Cl^- of 7, as reported in the literature [20]:

$$J_{eosm}(x) = n_h J_{tot}(x) \quad (12)$$

The net water transport through membranes is given by

$$J_w(x) = J_{osm}(x) + J_{eosm}(x) \quad (13)$$

Note that J_{osm} has been defined as a negative flux (eq. (11)), therefore the net water flux (J_w) in eq. (13) is an algebraic sum of two opposite contributions.

2.1.5 Mass balance in dilute-concentrate compartments

Mass balances for NaCl in both compartments have been developed taking into account also the effect of solvent transport on salt concentration [15]:

$$\frac{dC_{LOW}(x)}{dx} = \frac{b}{Q_{LOW}} J_{tot}(x) - C_{LOW}(x) \frac{b}{Q_{LOW}} J'_w(x) \quad (14)$$

$$\frac{dC_{HIGH}(x)}{dx} = -\frac{b}{Q_{HIGH}} J_{tot}(x) + C_{HIGH}(x) \frac{b}{Q_{HIGH}} J'_w(x) \quad (15)$$

where Q_{LOW}, Q_{HIGH} are the solution flow rates in each compartment, b is the membrane width, and J'_w is the volumetric flux of solvent through membranes (i.e. the molar flux from eq. (13), J_w , multiplied by the water molar density). Since the osmotic flux is higher than the electro-osmosis in these process conditions (i.e. using brine as concentrated solution), the net water flux is opposite to the salt flux, giving a further reduction of concentration in the concentrate compartment, as well as an increase in the dilute compartment.

2.1.6 Description of concentration polarisation phenomena

Following the cell pair voltage definition in eq. (4), the potential difference arising across each membrane depends on the actual salt concentration on membrane surface. Therefore, eq. (4) can be rewritten as:

$$E_{cell}(x) = (\alpha_{CEM} + \alpha_{AEM}) \frac{RT}{F} \ln \left[\frac{\gamma_{HIGH}^{int}(x) C_{HIGH}^{int}(x)}{\gamma_{LOW}^{int}(x) C_{LOW}^{int}(x)} \right] \quad (16)$$

where C^{int} is the real salt concentration at membrane-solution interface, γ^{int} is the mean activity coefficient of NaCl evaluated at interface concentration, subscripts *HIGH* and *LOW* refer to concentrate and dilute solutions, respectively. Note that the two terms on the

right-hand side of eq. (4) have been lumped together since the system contains only one symmetric electrolyte ($\gamma_+ = \gamma_- = \gamma_{\pm}$).

Polarisation phenomena lead to a change of the salt concentration at membrane-solution interface with respect to the bulk conditions. This is due to the ion transport through the membranes, which requires the same ions transport between the channel bulk and the interface. Such transport phenomena are, therefore, related to the generation of a gradient between bulk and interface, leading (in the case of the RED process) to a reduction the salt concentration on the HIGH-side and increases the salt concentration on the LOW-side of each membrane (Figure 4). As a result, the overall effect is a reduction of the available driving force for electric potential, which can be quantified defining ‘‘polarisation coefficients’’ as [24]:

$$\mathcal{G}_{HIGH} = \frac{C_{HIGH}^{int}}{C_{HIGH}^{bulk}} \quad \mathcal{G}_{LOW} = \frac{C_{LOW}^{bulk}}{C_{LOW}^{int}} \quad (17,18)$$

These coefficients can be seen as a measure of the effect of polarisation phenomena on the available driving force for the RED process (note that both \mathcal{G}_{HIGH} and \mathcal{G}_{LOW} are defined to be always ≤ 1).

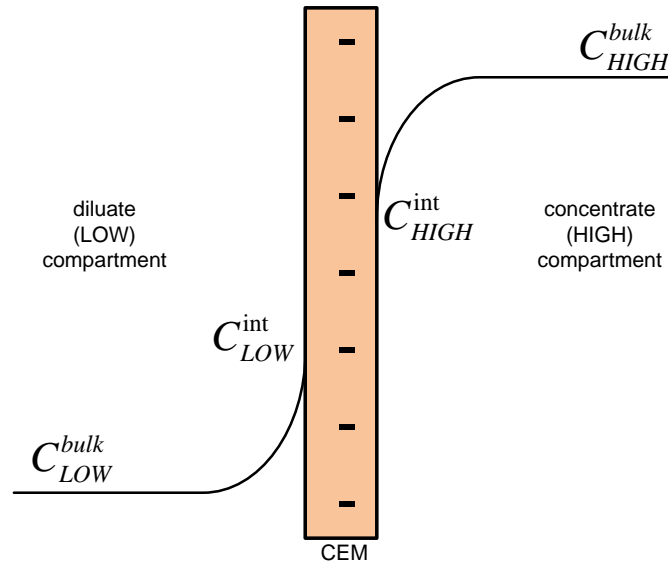


Figure 4. Schematic representation of concentration profiles close to a cationic membrane surface.

Substituting eq. (17,18) into eq. (16), the cell pair voltage becomes

$$E_{cell}(x) = (\alpha_{CEM} + \alpha_{AEM}) \frac{RT}{F} \ln \left[\mathcal{G}_{HIGH} \mathcal{G}_{LOW} \frac{\gamma_{HIGH}^{int}(x) C_{HIGH}^{bulk}(x)}{\gamma_{LOW}^{int}(x) C_{LOW}^{bulk}(x)} \right] \quad (19)$$

In order to calculate the polarisation coefficients, eq. (17,18) can be also written as:

$$\mathcal{G}_{HIGH} = \frac{C_{HIGH}^{int}}{C_{HIGH}^{bulk}} = \frac{C_{HIGH}^{bulk} - \Delta C_{HIGH}^*}{C_{HIGH}^{bulk}} \quad ; \quad \mathcal{G}_{LOW} = \frac{C_{LOW}^{bulk}}{C_{LOW}^{int}} = \frac{C_{LOW}^{bulk}}{C_{LOW}^{bulk} + \Delta C_{LOW}^*} \quad (20,21)$$

where ΔC_{HIGH}^* , ΔC_{LOW}^* are the concentration drops in the diffusion boundary layer for brine and seawater solutions, respectively. These quantities depend on the ionic flux through membranes (i.e. on the current density) as well as on the flow velocity inside channels. ΔC_{HIGH}^* , ΔC_{LOW}^* values were predicted by means of Computational Fluid Dynamics (CFD) simulations in a wide range of different operating conditions in order to get all the information necessary to implement eqs. (17-21) in the present model formulation [24, 25], as shown in Figure 5.

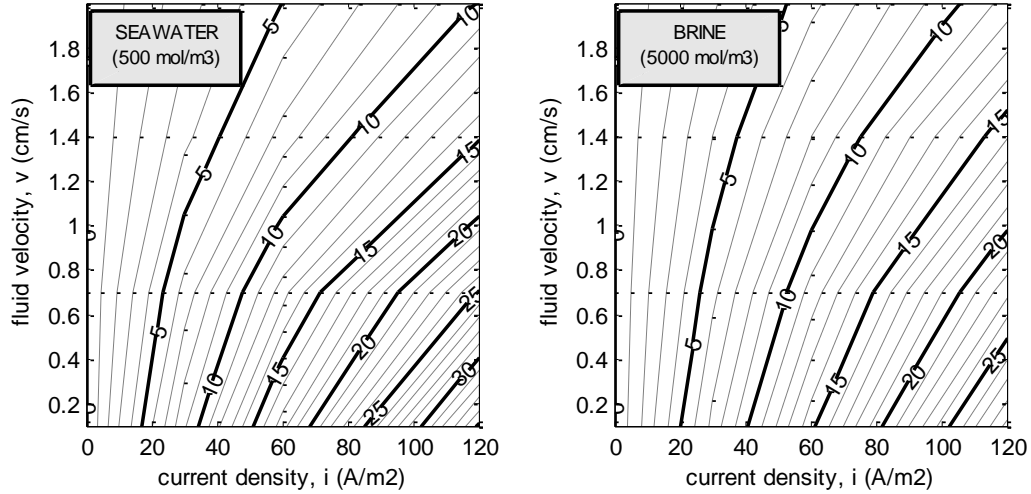


Figure 5. Effect of current density and fluid velocity on the concentration drop in diffusion boundary layer, ΔC_{HIGH}^* , ΔC_{LOW}^* (mol/m³). Case a) Seawater (0.5 M NaCl); case b) Brine (5 M NaCl). Model predictions from CFD simulations with 270 μ m polyamide woven spacer (Deukum GmbH, Germany) [24, 25].

The fluid velocity (v) in Figure 5 is defined as the mean feed flow velocity inside the spacer-filled channel and is equal to:

$$v = \frac{Q}{\delta b \varepsilon_{sp}} \quad (22)$$

where Q is the volumetric flow rate, δ is the spacer thickness, b is the channel width and ε_{sp} is the spacer porosity.

The concentration drop in the diffusion boundary layer (DBL) was estimated adding the correlations derived from CFD simulations (Figure 5) to the proposed model. Therefore, both polarisation coefficients were calculated by eq. (27,28) (Figure 6).

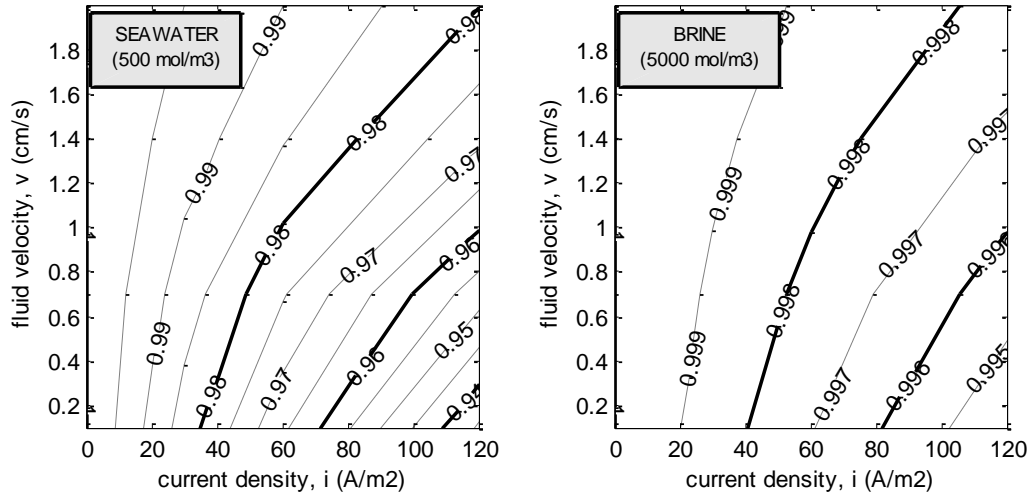


Figure 6. Effect of current density and fluid velocity on polarisation coefficients. Case a) Seawater (0.5 M NaCl); case b) Brine (5 M NaCl). Model predictions from CFD simulations with 270 μm polyamide woven spacer (Deukum GmbH, Germany) [24, 25].

It is worth noting that the concentration drop in DBL is quite similar for both solutions (Figure 5), with only slightly larger values predicted for the dilute solution (Figure 5.a). On the other side, the higher bulk concentration for the brine solution gives rise to a polarisation coefficient close to unity, i.e. negligibly affecting the cell potential (Figure 6.b).

2.2 High-hierarchy model (stack)

In the “stack” model, the system is constituted by a series of N cell pairs and two electrode compartments at the ends (Figure 2): the modelling goal at this level of description is to describe the interaction among the repeating units of the system (including also electrodes compartments and feed distribution/collection manifolds) in terms of electrical behaviour (current density, stack voltage), pressure drops and overall performance. Unlike the cell pair, which is modelled as a distributed system, in this section the system has been modelled as a lumped system, averaging each variable in the flow direction (x).

2.2.1 Cell pair current density and parasitic currents through manifolds

The electrical current, which can be collected from an external load, is essentially related to the salinity gradient-driven ion transport through the membranes. However, other “shortcut” paths can be imagined for ions to flow from high potential to low potential compartments: for instance, inlet and outlet manifolds are in fact “salt bridges” among cell pairs, which allow parasitic currents flowing through the stack dissipating part of the electrical energy generated inside the system. The effect of these parasitic currents may be described assuming an equivalent electrical circuit for the RED system, in which the cell pair is assumed as the repeating energy generation unit (including an “internal resistance”) and compartments and manifolds are the secondary electrical circuits. A graphical representation of the electrical circuit adopted herein is shown in Figure 7, based also on the circuit proposed by Veerman *et al.* [17].

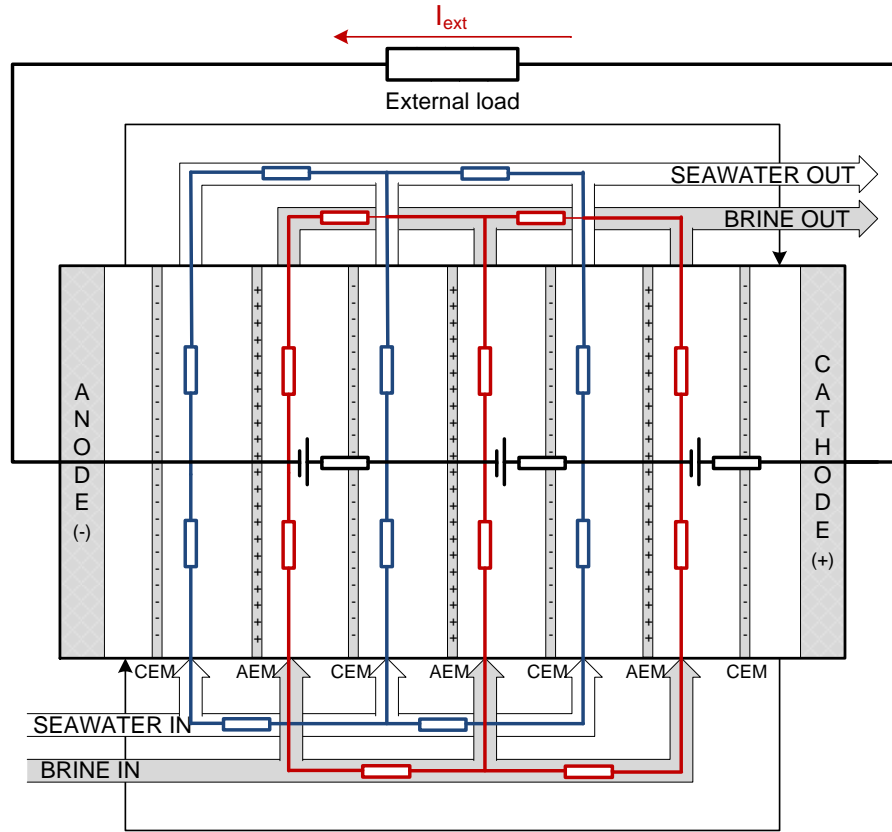


Figure 7. Equivalent circuit for parasitic currents in inlet/outlet manifolds and compartments. Black: main circuit; blue: parasitic currents in dilute solution (seawater) manifolds; red: parasitic currents in concentrate solution (brine) manifolds.

As shown in Figure 7, the parasitic currents in both compartments have been taken into account in the developed model.

The electrical resistance inside a generic k -th channel is evaluated by the following terms (Figure 8):

- electric resistance in HIGH/LOW solutions distributors (i.e. inlet manifolds):

$$R_{HIGH}^d = \frac{\delta_{tot}}{(\Lambda_{HIGH} C_{HIGH})_{x=0} S_d} \quad R_{LOW}^d = \frac{\delta_{tot}}{(\Lambda_{LOW} C_{LOW})_{x=0} S_d} \quad (23,24)$$

where δ_{tot} is the total distributor length between two subsequent compartments ($\delta_{tot} = \delta_{HIGH} + \delta_{LOW} + 2\delta_m$) and S_d is the cross-sectional area of the distribution channels, supposed as a rectangular channel.

- electric resistance in HIGH/LOW solutions collectors (outlet manifolds):

$$R_{HIGH,k}^c = \frac{\delta_{tot}}{(\Lambda_{HIGH,k}^c C_{HIGH,k}^c) S_c} \quad R_{LOW,k}^c = \frac{\delta_{tot}}{(\Lambda_{LOW,k}^c C_{LOW,k}^c) S_c} \quad (25,26)$$

In the equations above S_c is the cross-sectional area of collectors. The electrical resistance for the generic k -th compartment is a function of the salt concentration inside the collector ($C_{HIGH,k}^c, C_{LOW,k}^c$); this concentration can be estimated by a mass balance between two subsequent compartments:

$$Q_{HIGH,k}^c = Q_{HIGH,k} + Q_{HIGH,k+1}^c \quad Q_{LOW,k}^c = Q_{LOW,k} + Q_{LOW,k+1}^c \quad (27,28)$$

$$C_{HIGH,k}^c Q_{HIGH,k}^c = C_{HIGH,k} Q_{HIGH,k} + C_{HIGH,k+1}^c Q_{HIGH,k+1}^c \quad (29)$$

$$C_{LOW,k}^c Q_{LOW,k}^c = C_{LOW,k} Q_{LOW,k} + C_{LOW,k+1}^c Q_{LOW,k+1}^c \quad (30)$$

Rearranging the eq. (27-), the concentration inside the collector at the outlet of the k -th compartment is given by

$$C_{HIGH,k}^c = \frac{C_{HIGH,k} Q_{HIGH,k} + C_{HIGH,k+1}^c Q_{HIGH,k+1}^c}{Q_{HIGH,k} + Q_{HIGH,k+1}^c} \quad (31)$$

$$C_{LOW,k}^c = \frac{C_{LOW,k} Q_{LOW,k} + C_{LOW,k+1}^c Q_{LOW,k+1}^c}{Q_{LOW,k} + Q_{LOW,k+1}^c} \quad (32)$$

In order to take into account the concentration change along compartments, the relevant electric resistances were split in two contributions, investigating the difference from inlet ($x = 0$) to the centre ($x = L/2$), and from the centre to the outlet ($x = L$):

$$R'_{HIGH,k} = f_x \frac{L/2}{(\bar{\Lambda}'_{HIGH,k} \bar{C}'_{HIGH,k}) b \delta_{HIGH}} \quad (33)$$

$$R'_{LOW,k} = f_x \frac{L/2}{(\bar{\Lambda}'_{LOW,k} \bar{C}'_{LOW,k}) b \delta_{LOW}} \quad (34)$$

$$R''_{HIGH,k} = f_x \frac{L/2}{(\bar{\Lambda}''_{HIGH,k} \bar{C}''_{HIGH,k}) b \delta_{HIGH}} \quad R''_{s,k} = f_x \frac{L/2}{(\bar{\Lambda}''_{s,k} \bar{C}''_{s,k}) b \delta_s} \quad (35,36)$$

In these equations $\bar{\Lambda}'_{HIGH,k}, \bar{C}'_{HIGH,k}, \bar{\Lambda}'_{LOW,k}, \bar{C}'_{LOW,k}$ are mean variables evaluated between inlet-centre, while $\bar{\Lambda}''_{HIGH,k}, \bar{C}''_{HIGH,k}, \bar{\Lambda}''_{LOW,k}, \bar{C}''_{LOW,k}$ are evaluated between centre and outlet; f_x is a shadow factor calculated from the spacer open area in the flow direction, as will be explained in detail in the following paragraph.

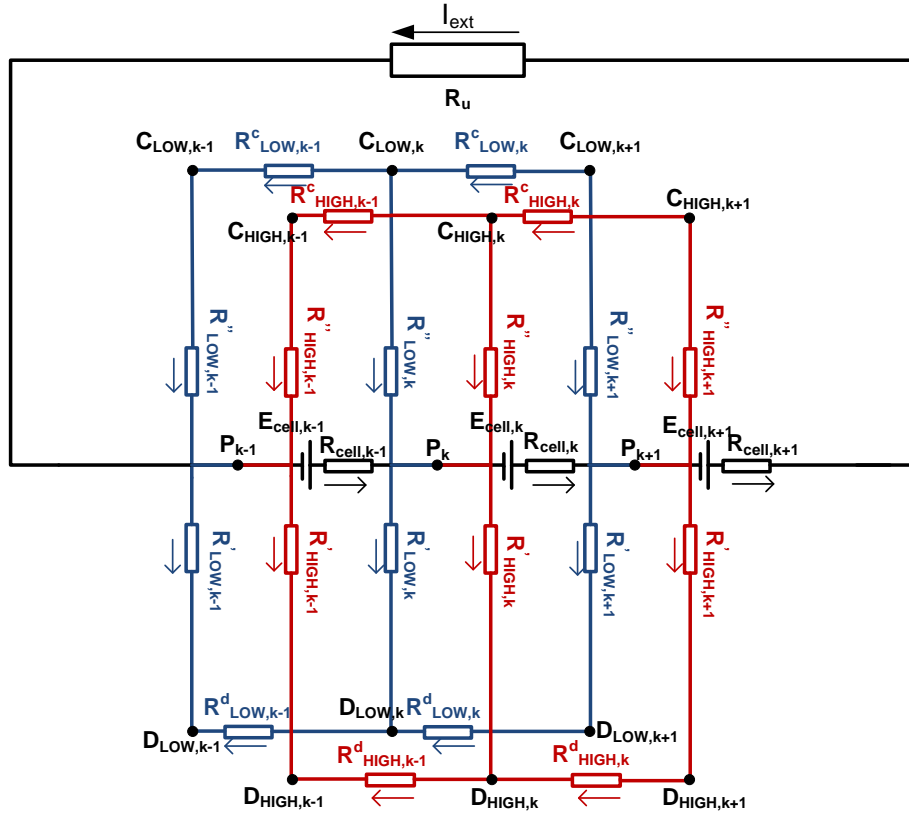


Figure 8. Equivalent circuit and electrical variables adopted for the prediction of parasitic currents in inlet/outlet manifolds and compartments.

Once the resistances shown in Figure 8 have been declared, the only equations involved for the evaluation of all the currents within each cell pair are Kirchhoff's law (eq. (37)) in the nodes (being the nodes indicated with P_k , $D_{s,k}$, $D_{b,k}$, $C_{s,k}$, $C_{b,k}$) and Ohm's law (eq. (38)) over all the resistances coupled with the Kirchhoff's law in the loops, where k is the cell pair number.

$$\sum_k I_k = 0 \quad R_k = \frac{\Delta V_k}{I_k} \quad (37,38)$$

It is worth noting that, in the equivalent electrical circuit (Figure 8) the concentrate and dilute compartments can be seen as converging towards a single node (P_k). This is, of course, not related to the real hydraulic circuits, in which the two channels are not converging into a common central point, but it is a simplification of the electrical circuit useful for the effective prediction of cell pair main current and parasitic currents phenomena.

2.2.2 Evaluation of the spacer shadow effect

The electrical resistances of dilute and concentrate solutions perpendicular to the membrane have been calculated by eq. (6,7), while the resistances along the channel are described in eq. (33-36). The open area of a specific spacer, which increases the electrical resistance, may be different in the direction perpendicular/along the membrane (Figure 9). For this reason, two different shadow factors have been defined based on the geometric features of the spacer:

$$f_x = \frac{1}{a_{open,x}} \quad f_y = \frac{1}{a_{open,y}} \quad (39,40)$$

Both $a_{open,x}$ and $a_{open,y}$ vary between a certain minimum value (i.e. on a plane containing the centre of filaments) and 100% (on a plane tangent to the filaments surface), while typical values for commercial spacers are 40-60%. This variation was taken into account assuming an average value for $a_{open,x}, a_{open,y}$.

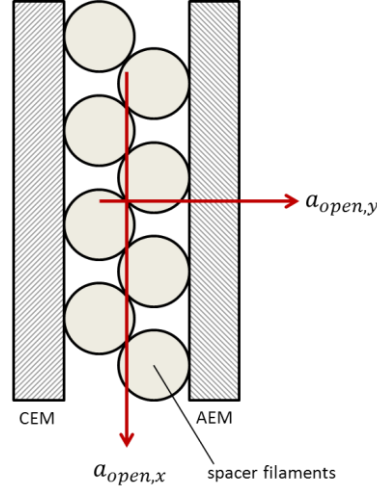


Figure 9. Spacer open area in direction perpendicular/parallel to the membrane.

2.2.3 Stack voltage and power density

The total stack resistance may be evaluated as:

$$R_{stack} = \left(\sum_{i=1}^N \bar{R}_{cell,i} \right) + R_{blank} \quad (41)$$

where R_{blank} is the resistance in the electrodes' compartments, which is estimated from experimental measurements.

The stack voltage is equal to the sum of all the electromotive force generated across each membrane pair (E_{cell}) minus the potential drop due to the internal cell resistance, for all cell pairs contained in the stack, minus the potential drop due to the electrodic compartments' resistance:

$$\bar{E}_{stack} = \sum_{i=1}^N \left(\bar{E}_{cell,i} - \bar{R}_{cell,i} \frac{\bar{I}_{cell,i}}{A} \right) - R_{blank} \frac{I_{ext}}{A} \quad (42)$$

Where $I_{cell,i}$ is the electric current flowing in the cell pair and I_{ext} is the electrical current collected in the external load, given by:

$$I_{ext} = \frac{\bar{E}_{stack}}{R_t} A \quad (43)$$

In eq. (43) R_u is the external load of the system (assumed as constant), multiplied by the cell pair area, in order to be expressed in Ωm^2 , thus being dimensionally consistent with all the other areal resistances defined within the model.

Finally, the specific power per cell pair area (power density) is evaluated as:

$$P_d = \frac{1}{N} \left(\frac{I_{ext}}{A} \right)^2 R_u \quad (44)$$

It is worth noting that the above defined power density refers to m^2 of cell pair, while in some other literature works it is defined per m^2 of total membrane.

2.2.4 Pressure drops

Pressure drops for the salt solutions inside the stack can be split into two main contributions:

- concentrated pressure drops, related to the manifolds and inlet/outlet sections of each compartment; this term is strongly dependent on the stack geometry and somehow also to spacer thickness and shape (for inlet/outlet drops);
- distributed pressure drops, which depend on the spacer geometry and are typically proportional to the flow velocity (assuming a laminar flow regime).

A detailed analysis of the fluid flow behaviour inside spacer-filled channels has been already performed using Computational Fluid Dynamics (CFD) modelling and presented by Gurreri *et al.* [24] and is beyond the scope of the present paper. However, in order to have an estimate of the pressure drops to evaluate the required pumping power of the system, both distributed and concentrated pressure drops for dilute and concentrate solutions were experimentally measured [25] inside a channel filled with a 270 μm polyamide woven spacer (Deukum GmbH, Germany) (Figure 10). The regression laws from fitting of the experimental data at different fluid velocity were added to the model.

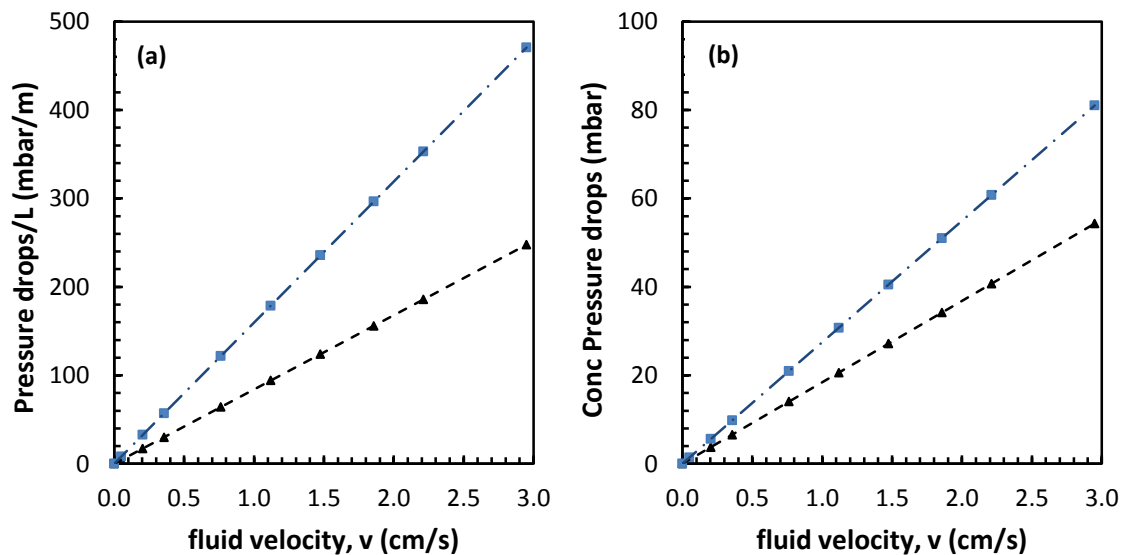


Figure 10. Distributed (a) and concentrated (b) pressure drops for a channel filled with Deukum 270 μm polyamide woven spacer. Experimental measurements performed inside a single channel using pure water (▲) and 4 M NaCl solution as brine (■).

The required power for pumping the salt solutions through the stack is calculated by:

$$P_{pump} = \frac{\Delta P_{HIGH} Q_{HIGH}^{tot} + \Delta P_{LOW} Q_{LOW}^{tot}}{\eta_p} \quad (45)$$

where ΔP is the total pressure drop, Q^{tot} is the flow rate of both solutions, and η_p is pump efficiency (set by default to 75%); subscripts *HIGH* and *LOW* refer to concentrate and dilute solution, respectively.

Finally, the performance of the RED process can be evaluated through the net power density, i.e. the obtainable electric power normalised for the cell pair area after the subtraction of the pumping power:

$$P_{d,net} = P_d - \frac{P_{pump}}{NA} \quad (46)$$

Note that in eq. (46) the pumping power (P_{pump}) has been divided by the cell pair area (NA) to be dimensionally consistent with the power density.

The final set of equations (eq. (1)-(46)) were eventually implemented into in an equation-based process simulator (gPROMS®). The developed model has been afterwards tuned and validated by comparison with experimental data, as will be described in paragraph 3.

3 Model calibration and validation procedure

3.1 Experimental setup

Experimental data used for calibration were collected during an extensive experimental campaign performed at VITO (Flemish Institute for Technological Research, Mol – Belgium) within the activities of the REAPower project [26]. A newly designed lab-scale stack (provided by REDstack BV, The Netherlands) with a cross-flow configuration (50 cell pairs with 10x10 cm² of active membrane area) was used for collecting experimental data to validate the model.

It is worth noting that, although the model has been implemented for a co-current flow distribution, the experimental data collected with the cross-flow stack can be effectively used for calibration. In fact, given the small residence time and negligible variation of streams properties along compartments, no significant difference can be found between the two operating configurations.

The electrode compartments consisted of two Ru-Ir mixed metal oxide electrodes (Magneto Special Anodes BV, The Netherlands) rinsed by a 0.1 M $K_3Fe(CN)_6 / K_4Fe(CN)_6$ aqueous solution with 2.5 M NaCl as supporting electrolyte. These species give good performance and high stability under the operating conditions of the RED process [27, 28].

The stack was equipped with a 270 μm polyamide woven spacer (Deukum GmbH, Germany) and Fujifilm ion-exchange membranes (Fujifilm Manufacturing Europe BV, The Netherlands), purposely developed to be used with highly concentrated salt solutions. The relevant physical properties of IEMs are listed in Table 1.

Table 1 Physical properties of Fujifilm ion exchange membranes [29].

Membrane	Thickness, μm	Permselectivity (0.5 M - 4 M)	Hydraulic permeability, $\text{ml}/\text{bar h m}^2$
AEM 80045-01	120	0.65	4.96
CEM 80050-04	120	0.90	4.72

Peristaltic pumps (Hosepump Masterflex PW, Burt Process Equipment Inc., USA) were used for circulating both salt solutions, as well as the electrode rinse solution. Experimental measurements were carried out using a galvanostat (Autolab PGSTAT100, Metrohm, USA). The salt solutions were made using distillate water and technical grade NaCl (Frisia Salt, The Netherlands).

3.2 Experimental measurements

Experimental measurements consisted of voltammetric analyses in galvanostatic mode: each measurement was performed imposing a change in the external current in the range 0–0.3 A with a step of $0.5 \text{ mA}/\text{s}$, measuring the voltage difference at stack terminals. Hence, the stack resistance and the electric power can be calculated by Ohm's laws. In order to validate the proposed model in a wide range of operating conditions, experimental measurements were performed changing the concentration of either the dilute (LOW) or the concentrate (HIGH) streams, the fluid velocity of the two solutions inside the stack channels and the feeds inlet temperature, as summarised in Table 2.

Table 2. Experimental measurements used for model tuning/validation.

Experiment goal	HIGH conc, mol/l	LOW conc, mol/l	feed flow velocity, cm/s	Temperature, $^{\circ}\text{C}$
Influence of concentration of the dilute feed (LOW)	5.0	1.0 0.9 0.7 0.5 0.3 0.1	1.0	20
Influence of concentration of the concentrate feed (HIGH)	5.0 4.0 2.86 1.96 1.0	0.55	1.0	20
Influence of feed flow velocity	5.0	0.5	0.5 0.7 1.0 2.0 4.0	20
Influence of feed temperature	5.0	0.5	1.0	20 30 40

The actual experimental information collected by the measuring instrument is the stack voltage (E_{stack}). Therefore, such variable has been taken into account for model fitting, as will be described in detail in the next section.

3.3 Definition and calibration of tuning parameters

The procedure adopted for the model tuning is sketched in Figure 11. During the experimental measurements the galvanostat fixed the external current under certain conditions and measured the corresponding stack voltage; therefore, the same values of current imposed by the galvanostat has been used as input data for the model. Finally, simulations were run by the process simulator, evaluating the values of the tuning parameters, which minimise the discrepancy between model predictions and experimental results.

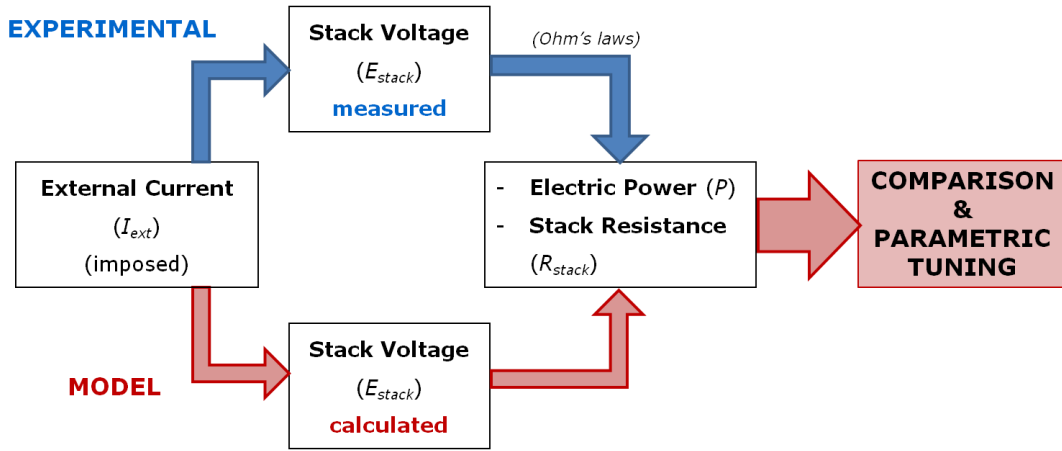


Figure 11. Logic scheme of the procedure adopted for model validation.

The best values of the tuning parameters were determined evaluating the discrepancy with experiments using a robust objective function (*Maximum Likelihood estimation* [30]). The tuning parameters were chosen in order to evaluate the membrane properties under different feed concentration conditions. In particular, two different parameters were used:

- *permselectivity correction factor* (β):

$$E_{cell}(x) = \beta(\alpha_{CEM} + \alpha_{AEM}) \frac{RT}{F} \ln \left[\mathcal{G}_b \mathcal{G}_s \frac{\gamma_b(x) C_b(x)}{\gamma_s(x) C_s(x)} \right] \quad (47)$$

defined to take into account the non-ideal behaviour of the system in terms of cell pair voltage (e.g. the effect of high salt concentration on IEM permselectivity);

- *resistance correction factor* (f_m): this factor accounts for the effect of solutions concentration on IEMs. Consequently, the effective IEMs resistances were evaluated as:

$$R_{AEM,eff} = f_m R_{AEM} \quad R_{CEM,eff} = f_m R_{CEM} \quad (48,49)$$

Finally, a parametric variation study was performed, in order to point out the dependence of β and f_m on the two solutions concentration.

Experimental measurements carried out changing the LOW/HIGH concentration (Table 3) were used for the model calibration, in order to find the effect of salt concentration on the tuning parameters. The overall input data used for model calibration are reported in Table 3.

Table 3. Parameters used for model calibration.

stack design		unit	CF
cell pair	Number of cell pairs, N	-	50
	membrane width, b	cm	9.5
	membrane length, L	cm	9.5
solutions	HIGH inlet concentration, C_{HIGH}	mol/l	1 – 5 M
	LOW inlet concentration, C_{LOW}	mol/l	0.1 – 1 M
	feed flow velocity, single channel	cm/s	1.0
membranes [29]	CEM permselectivity, α_{CEM}	-	0.9
	AEM permselectivity, α_{AEM}	-	0.65
	CEM resistance, R_{CEM}	$\Omega \cdot \text{cm}^2$	2.96
	AEM resistance, R_{AEM}	$\Omega \cdot \text{cm}^2$	1.55
	AEM-CEM thickness, δ_m	μm	125
	AEM-CEM water permeability, L_p	ml/bar·h·m ²	4.84
spacer	spacer thickness, δ	μm	270
	mesh opening	μm	600
	wire diameter	μm	150
	open area, in the direction perpendicular to membrane	-	0.64
	open area, in the direction of feed flow	-	0.36
	relative spacer volume	-	0.175
	shadow factor perpendicular to membrane, f_y	-	1.212
	shadow factor parallel to the membrane, f_x	-	1.471

Using the aforementioned parameters for the calibration, suitable values of tuning parameters were obtained. A parametric variation study was performed, in order to register the variation of these parameters with the concentration and, eventually, finding a reasonably linear trend. As a result, the following correlations were worked out, expressing the tuning parameters as a function of the inlet concentration of both solutions:

$$\beta = 1.212 - 0.281C_{LOW} - 0.086C_{HIGH} \quad (50)$$

$$f_m = 0.850 - 0.091C_{LOW} - 0.052C_{HIGH} \quad (51)$$

Finally, eqs. (46)-(47) have been added to the model and simulations repeated to make a comparison with the experimental results (Figure 12).

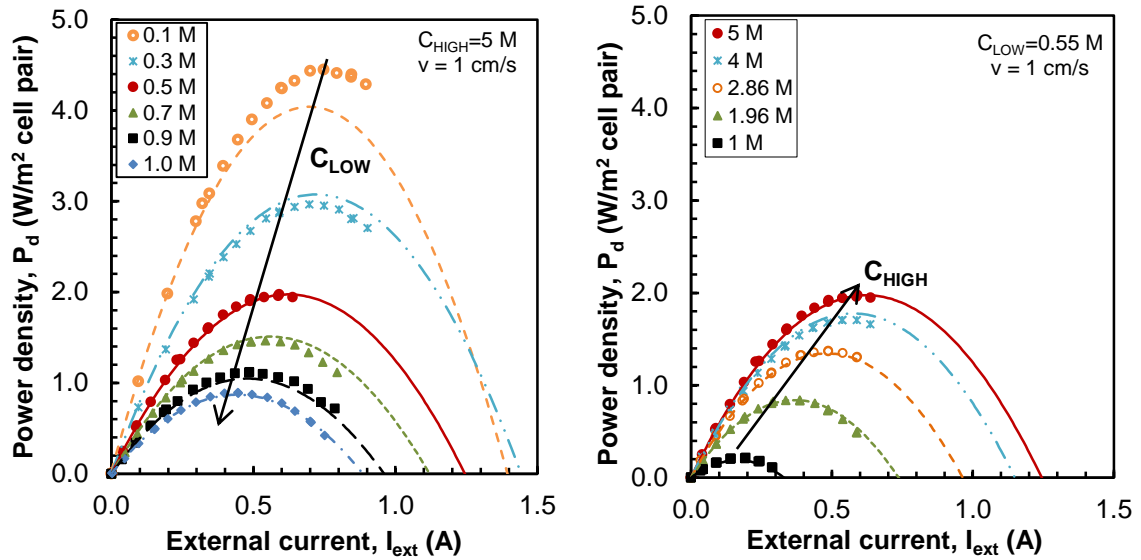


Figure 12. Effect of the inlet concentration on power density. Experimental (points) and simulated (lines) data for a 50 cell pairs stack (10×10 cm² membrane active area) equipped with Fujifilm membranes, 270 μ m woven spacers. Feed flow velocity: 1 cm/s; $T=20^\circ\text{C}$. Case a) changing LOW concentration ($C_{HIGH}=5$ M); case b) changing HIGH concentration ($C_{LOW}=0.55$ M).

The good accordance between experimental and predicted data in Figure 12 show that the model can be used as a predictive tool in a wide range of concentrations. Therefore, a further validation step has been carried out under different conditions of feeds flow rate and feeds temperature.

3.4 Model sensitivity towards the fixed salt permeability coefficient

Regarding the assumption of a fixed value of NaCl permeability coefficient (D_{NaCl}), the sensitivity of the model towards this parameter has been investigated in order to assess how such a choice could affect the model reliability and robustness. Model output within a wide range of variation of D_{NaCl} (from 10^{-13} up to 10^{-11} m²/s) was analysed, for fixed standard operating conditions (Figure 13).

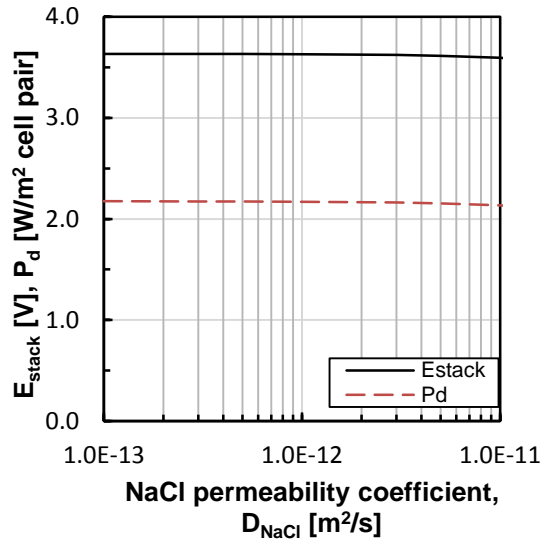


Figure 13. Effect of NaCl permeability coefficient on stack voltage and power density. Simulations of a 50 cell pairs stack ($10 \times 10 \text{ cm}^2$ membrane active area) equipped with Fujifilm membranes, $270 \text{ }\mu\text{m}$ woven spacers. CHIGH=5 M; CLOW=0.5 M; feed flow velocity: 1 cm/s.

Figure 13 shows how model predictions are not affected by the variation of D_{NaCl} , even though the two orders of magnitude range of variation investigated. As a result, fixing the value of $D_{NaCl} = 10^{-12} \text{ m}^2 / \text{s}$ is a reliable assumption, which does not affect the model prediction capability. This is in accordance with physical expectations, as in such highly permselective IEMs diffusion phenomena of co-ions are normally “minor” transport phenomena compared to the dominant transport phenomena of counter-ions.

4 Model Predictions and Results

4.1 Influence of feed flow rate

In order to further confirm the model prediction capabilities, also the effect of feed flow rates on process performance has been investigated and results compared with collected experimental information. In agreement with experiments, a concentration of 0.5 M NaCl and 5 M NaCl has been chosen for dilute and concentrated streams, respectively. Figure 14 shows the model predictions for the maximum power density achieved as a function of feed flow velocity inside a single compartment, as well as the experimental results collected in the same conditions.

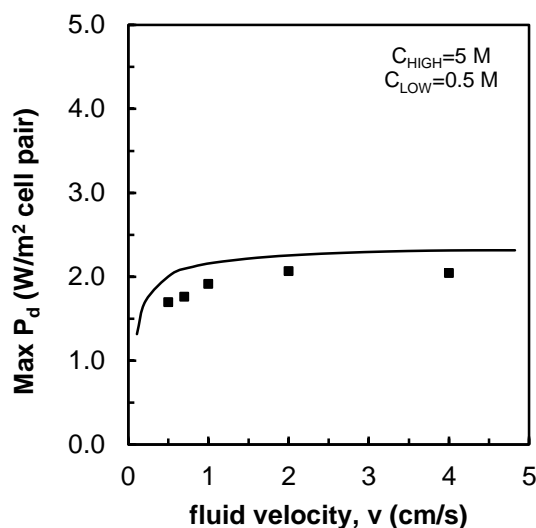


Figure 14. Effect of feed flow velocity on max power density. Experimental (points) and simulated (lines) data for a 50 cell pairs stack ($10 \times 10 \text{ cm}^2$ membrane active area) stack equipped with Fujifilm membranes, $270 \text{ }\mu\text{m}$ woven spacers. $C_{\text{HIGH}} = 5 \text{ M}$; $C_{\text{LOW}} = 0.5 \text{ M}$; $T = 20^\circ\text{C}$.

Model predictions clearly show how the velocity plays a role, especially in the lower part of the investigated range, where a strong non-linearity is observed. The trend shows, in fact, an increase in the maximum power density until a plateau is reached, as already pointed out in a recent literature study [31]. Such behaviour is in agreement with physical expectations, as lower velocities can dramatically increase the residence time, thus leading to a larger variation of streams concentration and, subsequently, a reduction in the process driving force. Such dependence is even more enhanced due to polarisation phenomena, which are almost negligible for larger velocities, while they can reduce the effective driving force across the membrane for lower ones [24, 32].

4.2 Influence of feed temperature

Temperature can also affect significantly the transport properties of both membranes and solutions. In particular, the influence of increasing temperature on membrane resistance was experimentally observed by means of Electrochemical Impedance Spectroscopy (EIS) measurements [23]. The experimental information provided by the EIS measurements was implemented into the model to investigate the influence of temperature on system performance, being the model able to predict also the influence of T on other variables such as cell potential, solutions properties, etc. Results are shown in Figure 15, where the maximum power density reached by a 50-cell pairs stack is reported as a function of the feed temperature of both solutions.

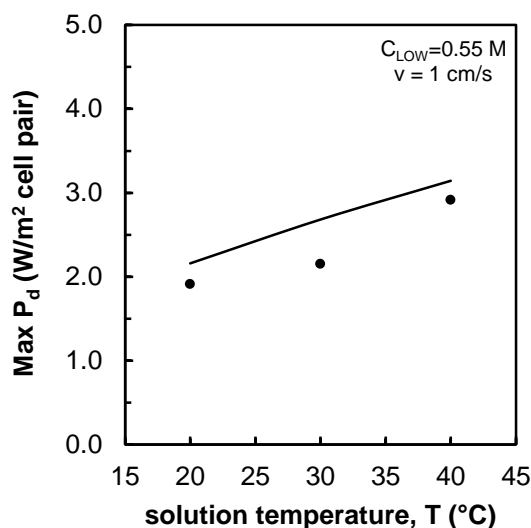


Figure 15. Effect of solution temperature on max power density. Experimental (points) and simulated (lines) data for a 50 cell pairs stack (10x10 cm² membrane active area) equipped with Fujifilm membranes, 270 μm woven spacers. C_{HIGH} = 5 M; C_{LOW} = 0.5 M; feed flow velocity: 1 cm/s.

Increasing the feed temperature has a positive effect on the conductivity of solutions and on ions mobility through the membranes, thus significantly reducing the overall resistance of the stack, as already mentioned in [23]. In agreement with these considerations, Figure 15 clearly shows how the increase of temperature can notably enhance the process performance. In particular, increasing the temperature from 20 to 40°C, the model predicts a 45% increase of the maximum power density. The same trend were previously found by other authors, though those data referred to different experimental conditions, especially in terms of feed concentration [33, 34]. This influence is particularly interesting for those applications in which the salt solutions are already available at a temperature higher than 20°C, such as the case of using concentrated brines and seawater from saltworks.

4.3 Optimal feed conditions for maximum P_d

The choice of salt concentration of dilute/concentrated solutions is a crucial issue for the RED process optimisation. In principle, the higher the salinity gradient between dilute-concentrate, the higher is the driving force for power production. On the other hand, this relation is not the only one controlling the process power output due to the effect of salt concentration on solution properties (e.g. activity coefficients, conductivity) and membrane properties (permselectivity, resistance). The validated model has been used to predict the maximum power output obtained when different salt solutions are used, ranging from river water to seawater (0.01 – 0.55 M NaCl) as a dilute, and from seawater to brine (0.5 – 5 M NaCl) as a concentrate. A P_d distribution map is shown in Figure 16.

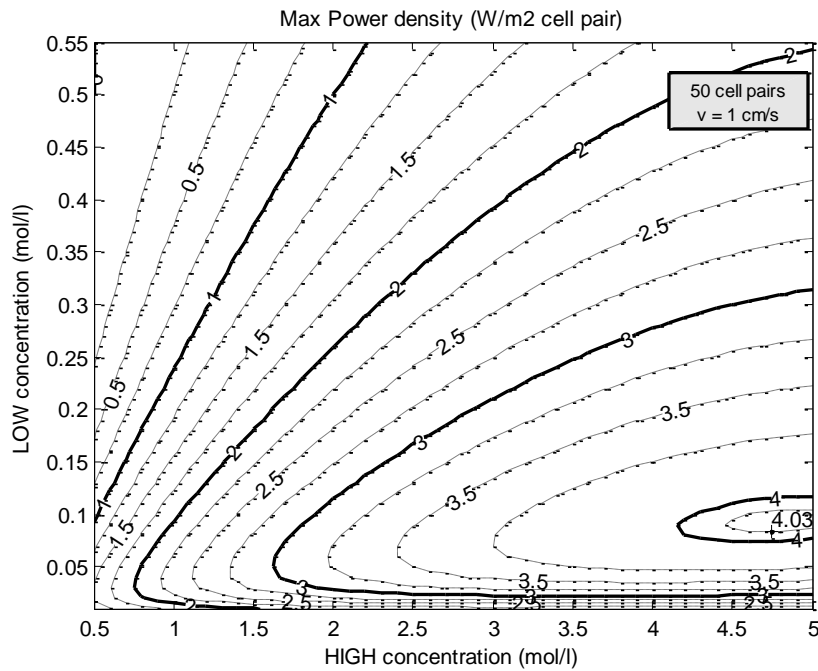


Figure 16. Effect of LOW/HIGH inlet concentration on maximum power density. Simulations of a 50 cell pairs stack ($10 \times 10 \text{ cm}^2$ membrane active area) equipped with Fujifilm membranes, $270 \text{ }\mu\text{m}$ woven spacers; feed flow velocity inside channels: 1 cm/s . $T=20^\circ\text{C}$. Contours show max power density (W/m^2).

Looking at Figure 16, the maximum power density predicted by the model for a 50 cell pairs stack is around 4 W/m^2 cell pair: this value can be achieved using a 80-100 mM NaCl solution as dilute (typical of brackish water) and 4.5-5 M NaCl solution as concentrate. It is worth noting that a further decrease of the dilute concentration can lead to a significant increase of the stack resistance. This would reduce the maximum power achievable, in spite of the higher concentration difference available within the RED stack. Furthermore, increasing the feed temperature from 20°C up to 40°C a 30% increase in the maximum power density can be achieved. This result is shown in Figure 17, where the maximum P_d is plotted as a function of dilute feed concentration at three different values of feed temperature and fixing brine concentration to 4.8M, i.e. the value maximising the P_d at 20°C (Figure 16). Interestingly, a power density of 5.3 W/m^2 is reached for the case of 40°C and 0.11M feed concentration.

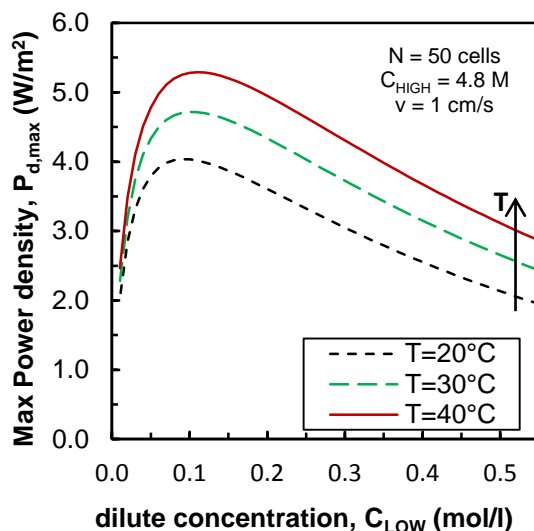


Figure 17. Simulations of 50 cell pairs stack ($10 \times 10 \text{ cm}^2$ membrane active area) equipped with Fujifilm membranes, $270 \text{ }\mu\text{m}$ woven spacers; feed flow velocity inside channels: 1 cm/s ; $C_{\text{HIGH}}=4.8 \text{ M}$.

5 Conclusions

The aim of this work has been to propose a new model for the RED process using sea or brackish water and concentrated brine as feed solutions. The physical properties of solutions, i.e. activity/osmotic coefficients, equivalent conductivity, density, etc., were estimated by means of correlations from the relevant literature; transport equations were implemented for both salt (counter-ions/co-ions) and solvent (osmotic and electro-osmotic fluxes). The effect of parasitic currents along the distributor/collector was estimated assuming an equivalent electrical circuit for both solutions; finally, the effect of polarisation phenomena has been taken into account evaluating the concentration drop in the diffusion boundary layer through Computational Fluid Dynamics simulations.

The developed model has been implemented in an equation-based process simulator (gPROMS®) in order to calibrate it on experimental data and to build eventually a simulator for the RED process.

Using two tuning parameters to take into account the influence of feed concentration on the most relevant membranes properties (permselectivity and resistance), the model was able to predict fairly well the experimental behaviour for a wide range of operating conditions (inlet concentrations, flow rates, feed temperature).

After the tuning/validation task, the proposed model was used to predict the effect of different inlet concentrations on process performance. With this regard, the best choice with the investigated stack membranes and geometry has been found to be the use of brackish water ($0.08\text{-}0.1 \text{ M NaCl}$) as dilute and brine ($4.5\text{-}5 \text{ M NaCl}$) as concentrate, which would lead to a maximum power density of more than 5 W/m^2 cell pair for a 50 cell pairs stack at 40°C .

The proposed model will be used as a design tool for the proper scale-up of the RED technology, also performing wider sensitivity analysis aiming at the development of a pilot-scale RED unit. Moreover, this will allow to explore the potentials for improvement and orient further R&D efforts towards new technological breakthroughs, which might

lead in the near future the RED process to play a dominant role among novel renewable energy technologies.

Acknowledgements

This work has been performed within the REAPower (Reverse Electrodialysis Alternative Power production) project [11], funded by the EU-FP7 programme (Project Number: 256736). The authors acknowledge the colleagues Etienne Brauns, Joost Helsen, Paolo Modica and Giuseppe Russo, and VITO Research Center for providing the experimental information adopted for the model validation.

Nomenclature

Latin letters

$a_{open,x}$	spacer open area in the direction along IEM (-)
$a_{open,y}$	spacer open area in the direction perpendicular IEM (-)
a	parameter of Islam et al.' equation (-)
A	membrane area or cell pair area, (m ²)
A_1	Debye-Hückel constant (0.3915 at 25°C)
b	channel (or membrane) width (m)
b'	constant of Pitzer equation (-)
B'	parameter of Islam et al.' equation, (m ^{1/2} mol ^{-1/2})
B'_1	parameter of Islam et al.' equation, (S m ³ mol ^{-3/2})
B'_2	parameter of Islam et al.' equation (m ^{3/2} mol ^{-1/2})
B''	second virial coefficient of Pitzer equation (kg mol ⁻¹)
B^φ	second virial coefficient of Pitzer equation (kg mol ⁻¹)
c	molar concentration (mol l ⁻¹)
C	salt concentration (mol m ⁻³)
$\bar{C}'_{HIGH,k}, \bar{C}'_{LOW,k}$	salt concentration averaged between inlet-centre of k-th channel
$\bar{C}''_{HIGH,k}, \bar{C}''_{LOW,k}$	salt concentration averaged between centre-outlet of k-th channel
C'	third virial coefficient of Pitzer equation (Kg ² mol ⁻²)
C^φ	third virial coefficient of Pitzer equation (Kg ² mol ⁻²)
D_{NaCl}	NaCl permeability coefficient (m ² s ⁻¹)
E_{cell}	cell pair voltage (V)
E_{stack}	stack voltage (V)
F	Faraday constant (96490 C mol ⁻¹)
f_y, f_x	spacer shadow factor in the direction perpendicular/along IEM (-)
f_m	shadow factor for membranes
F'	parameters of Islam et al.' equation (-)
I	electric current (A)
I'	ion strength (mol/l)
j	current density (A m ⁻²)
J'_w	volumetric water flux (m ³ m ⁻² s ⁻¹)
J_{tot}	salt molar flux (mol m ⁻² s ⁻¹)
J_{eosm}	electro-osmotic flux (mol m ⁻² s ⁻¹)
J_{osm}	osmotic flux (mol m ⁻² s ⁻¹)
J_w	net water flux (mol m ⁻² s ⁻¹)
L	channel length (m)
L_p	water permeability coefficient (m ³ ·bar ⁻¹ ·m ⁻² ·h ⁻¹)

m	electrolyte molal concentration (mol kg ⁻¹)
N	number of cell pairs (-)
P_d	gross power density (W m ⁻² cell pair)
$P_{d,net}$	net power density (W m ⁻² cell pair)
P_{pump}	pumping power (W)
Q_{HIGH}, Q_{LOW}	concentrate/dilute solution flow rate in single channel (m ³ s ⁻¹)
Q_{tot}	total feed flow rate (m ³ s ⁻¹)
R	universal gas constant (8.314 J mol ⁻¹ K ⁻¹)
R_{AEM}, R_{CEM}	AEM/CEM areal resistance (Ω m ²)
R_{HIGH}, R_{LOW}	concentrate/dilute compartment areal resistance (Ω m ²)
R_{blank}	electrode compartments (blank) resistance (Ω m ²)
R_{cell}	resistance of a single cell pair (Ω m ²)
R_{stack}	total stack resistance (Ω m ²)
R_u	external load (Ω m ²)
T	temperature (K)
v	fluid velocity (m s ⁻¹)
x	flow direction (m)
z	ion valence (-)

Greek letters

$\alpha_{AEM}, \alpha_{CEM}$	AEM/CEM permselectivity (-)
β	permselectivity correction factor (-)
γ_{\pm}	mean activity coefficient (-)
$\delta_{HIGH}, \delta_{LOW}$	HIGH/LOW compartment thickness (m)
δ_m	membrane thickness (m)
δ_{tot}	total cell pair thickness (m)
ϵ	dielectric constant (-)
ϵ_{sp}	spacer porosity (-)
ϕ	osmotic coefficient (-)
$\vartheta_{HIGH}, \vartheta_{LOW}$	polarisation coefficients (-)
ΔC_{HIGH}^*	concentration drops in the diffusion boundary layer for the concentrated solution
ΔC_{LOW}^*	concentration drops in the diffusion boundary layer for dilute solution
ΔP	pressure drop (Pa)
$\Delta \Pi^*$	real osmotic pressure difference (Pa)
η	viscosity of solution (Pa s)
η_p	pump efficiency (-)
υ	van't Hoff factor (-)
Λ	equivalent conductivity (S m ² mol ⁻¹)
Λ^0	equivalent conductivity at infinite dilution (126.5·10 ⁻⁴ S m ² mol ⁻¹)
$\bar{\Lambda}'_{HIGH,k}, \bar{\Lambda}'_{LOW,k}$	equivalent conductivity averaged between inlet-centre of k-th channel
$\bar{\Lambda}''_{HIGH,k}, \bar{\Lambda}''_{LOW,k}$	equivalent conductivity averaged between centre-outlet of k-th channel

Subscripts and superscripts

c	collector
cell	cell pair

d	distributor
ext	external circuit
LOW	diluted solution
HIGH	concentrated solution
bulk	bulk conditions
int	membrane-solution interface

Acronyms

AEM	Anionic Exchange Membrane
CEM	Cationic Exchange Membrane
IEM	Ion Exchange Membrane
RE or RED	Reverse Electrodialysis
SGP	Salinity Gradient Power
DBL	diffusion boundary layer
CFD	Computational Fluid Dynamics

References

- [1] R. E. Lacey, "Energy by reverse electro dialysis," *Ocean Engineering*, vol. 7, pp. 1-47, 1980.
- [2] R. E. Pattle, "Production of Electric Power by mixing Fresh and Salt Water in the Hydroelectric Pile," *Nature*, vol. 174, pp. 660-660, 1954.
- [3] J. W. Post, J. Veerman, H. V. M. Hamelers, G. J. W. Euverink, S. J. Metz, K. Nijmeijer, *et al.*, "Salinity-gradient power: Evaluation of pressure-retarded osmosis and reverse electro dialysis," *Journal of Membrane Science*, vol. 288, pp. 218-230, 2007.
- [4] D. Brogioli, "Extracting renewable energy from a salinity difference using a capacitor," *Physical review letters*, vol. 103, p. 058501(4), 2009.
- [5] B. B. Sales, M. Saakes, J. W. Post, C. J. N. Buisman, P. M. Biesheuvel, and H. V. M. Hamelers, "Direct power production from a water salinity difference in a membrane-modified supercapacitor flow cell," *Environmental Science and Technology*, vol. 44, pp. 5661-5665, 2010.
- [6] J. N. Weinstein and F. B. Leitz, "Electric power from differences in salinity: the dialytic battery," *Science (New York, NY)*, vol. 191, p. 557, 1976.
- [7] J. Jagur-Grodzinski and R. Kramer, "Novel process for direct conversion of free energy of mixing into electric power," *Industrial & Engineering Chemistry Process Design and Development*, vol. 25, pp. 443-449, 1986.
- [8] J. Veerman, M. Saakes, S. J. Metz, and G. J. Harmsen, "Reverse electro dialysis: Performance of a stack with 50 cells on the mixing of sea and river water," *Journal of Membrane Science*, vol. 327, pp. 136-144, 2009.
- [9] D. A. A. Vermaas, M. Saakes, and K. Nijmeijer, "Doubled Power Density from Salinity Gradients at Reduced Intermembrane Distance," *Environmental Science & Technology*, vol. 45, pp. 7089-7095, 2011.
- [10] E. Brauns, "Towards a worldwide sustainable and simultaneous large-scale production of renewable energy and potable water through salinity gradient power by combining reversed electro dialysis and solar power?," *Desalination*, vol. 219, pp. 312-323, 2008.
- [11] www.reapower.eu. Copyright 2010 REAPower/WIP Munich.
- [12] A. Cipollina, A. Misseri, G. D. Staiti, A. Galia, G. Micale, and O. Scialdone, "Integrated production of fresh water, sea salt and magnesium from sea water," *Desalination and Water Treatment*, vol. 49, pp. 390-403, 2012.
- [13] C. Forgacs, "Recent developments in the utilization of salinity power," *Desalination*, vol. 40, pp. 191-195, 1982.
- [14] E. Brauns, "Salinity gradient power by reverse electro dialysis: effect of model parameters on electrical power output," *Desalination*, vol. 237, pp. 378-391, 2009.
- [15] J. Veerman, M. Saakes, S. J. Metz, and G. J. Harmsen, "Reverse electro dialysis: A validated process model for design and optimization," *Chemical Engineering Journal*, vol. 166, pp. 256-268, 2011.
- [16] M. Tedesco, A. Cipollina, A. Tamburini, W. van Baak, and G. Micale, "Modelling the Reverse ElectroDialysis process with seawater and concentrated brines," *Desalination and Water Treatment*, vol. 49, pp. 404-424, 2012.
- [17] J. Veerman, J. W. Post, M. Saakes, S. J. Metz, and G. J. Harmsen, "Reducing power losses caused by ionic shortcut currents in reverse electro dialysis stacks by a validated model," *Journal of Membrane Science*, vol. 310, pp. 418-430, 2008.
- [18] K. S. Pitzer, "Thermodynamics of electrolytes. I. Theoretical basis and general equations," *The Journal of Physical Chemistry*, vol. 77, pp. 268-277, 1973.

- [19] S. Islam, R. Gupta, and K. Ismail, "Extension of the Falkenhagen-Leist-Kelbg equation to the electrical conductance of concentrated aqueous electrolytes," *Journal of chemical and engineering data*, vol. 36, pp. 102-104, 1991.
- [20] J. O. M. Bockris and A. K. N. Reddy, *Modern Electrochemistry vol. 1: Ionics*, 2nd ed.: Springer, 1998.
- [21] N. Lakshminarayanaiah, "Transport phenomena in artificial membranes," *Chemical reviews*, vol. 65, p. 491, 1965.
- [22] H. Strathmann, *Ion-exchange membrane separation processes* vol. 9: Elsevier Science Limited, 2004.
- [23] E. Fontananova, W. Zhang, I. Nicotera, C. Simari, W. van Baak, G. Di Profio, *et al.*, "Probing membrane and interface properties in concentrated electrolyte solutions," *Journal of Membrane Science*, in press (DOI 10.1016/j.memsci.2014.01.057), 2014.
- [24] L. Gurreri, A. Tamburini, A. Cipollina, G. Micale, and M. Ciofalo, "CFD simulation of mass transfer phenomena in spacer filled channels for reverse electrodialysis applications," *Chemical Engineering Transactions*, vol. 32, pp. 1879-1884, 2013.
- [25] G. Micale, A. Cipollina, A. Tamburini, and L. Gurreri, "Report on the CFD analysis of the effects of spacer filled channel geometry on the system performance," *REAPower project internal report*, 2012.
- [26] J. Helsen, P. Modica, and A. Cipollina, "Lab-scale SGP-RE stack testing: Small scale lab stack test results," *REAPower project internal report*, 2013.
- [27] O. Scialdone, C. Guarisco, S. Grispo, A. D. Angelo, and A. Galia, "Investigation of electrode material - Redox couple systems for reverse electrodialysis processes. Part I: Iron redox couples," *Journal of Electroanalytical Chemistry*, vol. 681, pp. 66-75, 2012.
- [28] O. Scialdone, C. Guarisco, S. Grispo, A. D. Angelo, and A. Galia, "Investigation of electrode material - Redox couple systems for reverse electrodialysis processes. Part II: Experiments in a stack with 10–50 cell pairs," *Journal of Electroanalytical Chemistry*, vol. 704, pp. 1–9, 2013.
- [29] "Fujifilm Manufacturing Europe BV, personal communication," ed.
- [30] P. Englezos and N. Kalogerakis, *Applied parameter estimation for chemical engineers* vol. 81: CRC, 2000.
- [31] J. G. Hong, W. Zhang, J. Luo, and Y. Chen, "Modeling of power generation from the mixing of simulated saline and freshwater with a reverse electrodialysis system: The effect of monovalent and multivalent ions," *Applied Energy*, vol. 110, pp. 244-251, 2013.
- [32] D. A. Vermaas, E. Guler, M. Saakes, and K. Nijmeijer, "Theoretical power density from salinity gradients using reverse electrodialysis," *Energy Procedia*, vol. 20, pp. 170-184, 2012.
- [33] A. Daniilidis, D. A. A. Vermaas, R. Herber, and K. Nijmeijer, "Experimentally obtainable energy from mixing river water, seawater or brines with reverse electrodialysis," *Renewable Energy*, vol. 64, pp. 123-131, 2014.
- [34] P. Długołęcki, A. Gambier, K. Nijmeijer, and M. Wessling, "Practical potential of reverse electrodialysis as process for sustainable energy generation," *Environmental Science and Technology*, vol. 43, pp. 6888-6894, 2009.
- [35] C. F. Weber, "Calculation of Pitzer Parameters at High Ionic Strengths," *Industrial & Engineering Chemistry Research*, vol. 39, pp. 4422-4426, 2000.

Appendix A

A.1 Calculation of Pitzer et al' parameters for activity coefficients evaluation

The Pitzer et al' correlation is a virial equation to estimate the activity coefficients in a wide range of solute concentration. The parameters presented in eq. (1) and (2) are defined as follows [18, 35]:

$$B^\gamma = 2\beta^{(0)} + 2\beta^{(1)} \left[1 - \left(1 + \alpha m^{1/2} - \alpha^2 m/2 \right) \exp(-\alpha m^{1/2}) \right] / \alpha^2 m \quad (\text{A1})$$

$$B^\varphi = \beta^{(0)} + \beta^{(1)} e^{-\alpha \sqrt{I}} \quad (\text{A2})$$

$$C^\gamma = \frac{3}{2} C^\varphi \quad (\text{A3})$$

where α is a fixed constant ($\alpha = 2 \text{ (kg/mol)}^{1/2}$); I' and m are the ion strength and molality of the electrolyte, respectively; $\beta^{(0)}$, $\beta^{(1)}$, C^φ are the adjustable parameters, which are function of the nature of the electrolyte and determined from fitting with experimental data. The values for NaCl are reported in Table A 1.

Table A 1. Binary interaction parameters of Pitzer equation for NaCl [35].

$\beta^{(0)}$	$\beta^{(1)}$	C^φ
0.06743	0.3301	0.00263

A.2 Calculation of Islam et al' parameters for equivalent conductivity evaluation

The Islam et al' correlation is an extension of the Falkenhagen-Leist-Kelbg (FLK) equation to estimate the equivalent conductivity of electrolyte solution at high concentration [19]. The extended definitions of parameters in eq. (3) are reported below:

$$B'(c) = 50.29 \cdot 10^8 / (\varepsilon T)^{1/2} \quad (\text{A4})$$

$$B_1'(c) = 82.5 / \left[\eta (\varepsilon T)^{1/2} \right] \quad (\text{A5})$$

$$B_2'(c) = 8.204 \cdot 10^5 / (\varepsilon T)^{3/2} \quad (\text{A6})$$

$$F' = \frac{\left[\exp(0.2929 B c^{1/2} a) - 1 \right]}{(0.2929 B c^{1/2} a)} \quad (\text{A7})$$

where a is the adjustable parameter used in the correlation to fit the experimental data ($a = 3.79 \text{ \AA}$ for NaCl); η , ε and T are viscosity, dielectric constant and temperature of the electrolyte solution, respectively.